ADVANCED MATERIALS
www.advmat.de

Extreme Water Uptake of Hygroscopic Hydrogels through Maximized Swelling-Induced Salt Loading

*Gustav Graeber, Carlos D. Díaz-Marín, Leon C. Gaugler, Yang Zhong, Bachir El Fil, Xinyue Liu, and Evelyn N. Wang**

Hygroscopic hydrogels are emerging as scalable and low-cost sorbents for atmospheric water harvesting, dehumidification, passive cooling, and thermal energy storage. However, devices using these materials still exhibit insufficient performance, partly due to the limited water vapor uptake of the hydrogels. Here, the swelling dynamics of hydrogels in aqueous lithiumchloride solutions, the implications on hydrogel salt loading, and the resulting vapor uptake of the synthesized hydrogel–salt composites are characterized. By tuning the salt concentration of the swelling solutions and the cross-linking properties of the gels, hygroscopic hydrogels with extremely high salt loadings are synthesized, which enable unprecedented water uptakes of 1.79 and 3.86 gg^{-1} at relative humidity (RH) of 30% and 70%, respectively. At 30% RH, this exceeds previously reported water uptakes of metal–organic frameworks by over 100% and of hydrogels by 15%, bringing the uptake within 93% of the fundamental limit of hygroscopic salts while avoiding leakage problems common in salt solutions. By modeling the salt-vapor equilibria, the maximum leakage-free RH is elucidated as a function of hydrogel uptake and swelling ratio. These insights guide the design of hydrogels with exceptional hygroscopicity that enable sorption-based devices to tackle water scarcity and the global energy crisis.

1. Introduction

Humanity faces important challenges related to the global supply of energy and water.[1,2] Efforts in energy and water have to be in line with the worldwide push toward net-zero emission strategies as well as adapt to constantly evolving environmental conditions in a rapidly changing climate. Research toward innovative, functional materials is a powerful means to address these challenges. One promising class of materials are sorbents. Sorption of water is commonplace in nature and widely used in a variety of technical processes that address water scarcity and enhance energy efficiency. These include freshwater production through atmospheric water harvesting,[3–7] passive thermal management,[8–12] thermal energy storage,[7,13–15] and space conditioning.[16,17] For sorbents to be good candidates for these applications, they need to be low-cost, scalable, and sustainable, as well as provide high water vapor uptake (i.e., high hygroscopicity), good sorption kinetics, low desorption enthalpies, and long-term cyclability. Finally, the sorbents must be easy to be integrated into the respective devices.

To meet these different requirements, many sorbent materials have been explored, including hygroscopic salts,[18–20] zeolites,[21–23] silicas,[24,25] and metal–organic frameworks (MOFs).[3,26,27] However, to date, there is no sorbent that can meet all the above criteria simultaneously. Hygroscopic hydrogels are an emerging class of sorbent materials with the potential of overcoming limitations present in other sorbents by providing extreme water uptakes, fast water capture and release kinetics, and low desorption enthalpies.[28–31] Hygroscopic hydrogels are typically synthesized by combining a hydrogel that possesses comparably low hygroscopicity with a sorbent component to substantially enhance hygroscopicity and form a composite material. The sorbent components range from salts,[10,32] MOFs,[33] to other hygroscopic polymers,[34] where previous literature has found that the hygroscopicity and mass loading of these components into the hydrogel are crucial to maximizing the water uptake.[30,35] In particular, due to the low-cost, commercial availability, and high hygroscopicity even at low relative humidity (RH), hygroscopic salts such as lithium chloride (LiCl) and calcium chloride are promising sorbent components.

Previous approaches to optimizing the mass loading of these sorbents into hydrogels include swelling the hydrogels in salt solutions with experimentally optimized concentrations, which has allowed loadings of 4 g of salt per g of polymer and a water uptake

G. Graeber[+], C. D. Díaz-Marín, L. C. Gaugler, Y. Zhong, B. El Fil, X. Liu, E. N. Wang
Department of Mechanical Engineering
Massachusetts Institute of Technology
Cambridge, Massachusetts 02139, USA
E-mail: enwang@mit.edu

The ORCID identification number(s) for the author(s) of this article can be found under https://doi.org/10.1002/adma.202211783

[+]Present address: Department of Chemistry, Humboldt-Universität zu Berlin, 12489 Berlin, Germany

DOI: 10.1002/adma.202211783

of 0.74 gg^{-1} at 35% RH.[32] Alternatively, polyzwitteronic hydrogels have been employed to enhance the salt loading via higher swelling ratios in concentrated salt solutions.[36,37] Hydrogels fabricated with this approach can achieve water uptakes of up to 0.62 gg^{-1} at 30% RH. In spite of these efforts, the hygroscopicity of these materials is not close to the fundamental limit of typical hygroscopic salts, which can be partially attributed to the limited loading of sorbents into the hydrogels during the swelling phase of the synthesis. Furthermore, beyond achieving high uptakes the hydrogel matrices should ensure containment of the salt solution as solution leakage can reduce the hydrogel performance over time and lead to device failure. To prevent leakage, previous works have explored hydrophobic encapsulations.[38] Alternatively, hydrogel swelling presents a simple alternative to prevent leakage with no additional need of materials.[32] Despite its promise, no previous works have elucidated the limits of this approach and its connection with the maximum water uptake achievable.

In this work, we combine the use of a highly hygroscopic sorbent such as LiCl with an unprecedented salt loading, which can exceed 20 g of LiCl per g of polymer, to achieve record high water uptakes of hygroscopic hydrogels. We performed prolonged (>50 days) swelling experiments of polyacrylamide (PAM) hydrogels in aqueous LiCl solutions with varying concentrations. Therefore, in contrast to previous works, we were able to fully decouple the equilibrium swelling ratio from the swelling kinetics and show that large swelling ratios are achievable despite high salt concentrations in the swelling solutions.[32] By modeling the swelling process, we found that the interaction between the polymer and the aqueous solution is most favorable for intermediate salt concentrations, while equilibrium swelling ratios are smaller at low salt concentration and close to saturation of the swelling solution. In contrast, the swelling kinetics become increasingly slower as the salt concentration increases, due to a lower effective diffusivity of the increasingly viscous solution into the polymer. By varying salt concentration and temperature of the swelling solution, cross-linking density of the hydrogel, drying protocols, and environmental sorption conditions, we established the fundamental relationship between swelling, salt loading, water uptake, and leakage in hygroscopic hydrogels. In contrast to previous attempts to predict salt leakage, here, based on our mechanistic insights, we provide guidelines for the optimization of leakage-free uptake also considering the effect of hydrogel swelling.[29,39] These guidelines enable the fabrication of LiCl-loaded PAM hydrogels with superior water uptake relative to the mass of dry sorbent (salt and polymer) of 1.79, 2.58, and 3.86 gg^{-1} at a RH of 30%, 50%, and 70%, respectively, exceeding previously reported water uptakes of MOFs[40,41] by over 100% and that of hydrogels by 15% even at arid conditions (30% RH).[42] These results bring the water uptake of hygroscopic hydrogels within 93% of the water uptake achievable with the best performing hygroscopic salts, while still avoiding leakage of salt solution even at humidities as high as 70%. This work represents a significant step in the successful integration of hygroscopic hydrogels for numerous water and energy applications such as atmospheric water harvesting, passive cooling, thermal energy storage, and space conditioning.

2. Results and Discussion

2.1. Material Synthesis

We synthesized PAM hydrogels based on a simple, one-pot approach by mixing deionized water, acrylamide monomer, *N,N'*-methylenebisacrylamidecrosslinker, ammonium persulfate initiator and *N,N,N′,N′*-tetramethylethylendiamin accelerator (see Experimental Section for details). We filled the pre-gel solution into capped vials to cure. After gelation, we cut the gel into thin disks as shown in **Figure 1**a. When fully swollen in deionized water (DIW), the disks have a diameter, L, of ≈25 mm, while their thickness, H, is ≈3 mm. After synthesis, we dried the disks for 3 days at 60 °C in an oven at an RH of ≈0%, which caused the disks to lose the majority of their mass and shrink substantially, as shown in Figure 1b. As sketched in Figure 1c, we studied free swelling of these initially dry hydrogel disks in aqueous LiCl solutions with different degrees of saturation $\%_{sat}$, ranging from pure DIW ($0\%_{sat}$) to LiCl-solutions with $25\%_{sat}$, $50\%_{sat}$, $75\%_{sat}$, and $100\%_{sat}$, corresponding, respectively, to concentrations of 0.172, 0.294, 0.384, and 0.454 g of salt per g of solution (reference temperature: 20 °C). As part of the swelling process in the salt solutions, the gels gained substantial weight as both water and solvated Li^+ and Cl^- ions diffuse into the nanoporous network of the gel (Figure 1d,e).

2.2. Swelling Dynamics of PAM in Aqueous LiCl Solutions

In **Figure 2**, we present our experimental measurements of the swelling process at room temperature (23 °C) along with our modeling results. Figure 2a shows the hydrogel swelling ratio as a function of swelling time. The swelling ratio is defined as the current sample weight at a given time of the experiment divided by the initial, dried sample weight as measured before placing the dried PAM disk in the aqueous LiCl solution. The swelling time is the time that has passed after the start of the swelling experiment, that is, the duration that the hydrogel had time to swell in the aqueous solution. To understand the effect of LiCl concentration in the aqueous solution, we performed swelling experiments in five different aqueous LiCl solutions. We found that the amount of LiCl in the aqueous solution affects both the equilibrium swelling ratio and the swelling kinetics. Most notably, large swelling ratios are achievable despite high salt concentrations. In fact, all tested concentrations of LiCl increased the swelling ratio with respect to pure DIW, indicating an energetically more favorable interaction between salt solution and PAM, relative to that of water and PAM.[43] We note that this result is distinct from previous works that reported the opposite trend where swelling was stopped after 48 h before reaching equilibrium.[37] This different outcome shows the importance of decoupling equilibrium uptake and kinetics. While swelling in pure DIW ($0\%_{sat}$) yielded a swelling ratio of 45, swelling ratios above 70 could be obtained in a $50\%_{sat}$ LiCl solution. However, further increasing the amount of LiCl revealed a non-monotonic relation between swelling ratio and LiCl concentration and reduced the equilibrium swelling ratio to ≈53 for the $100\%_{sat}$ LiCl solution. Given that the goal of

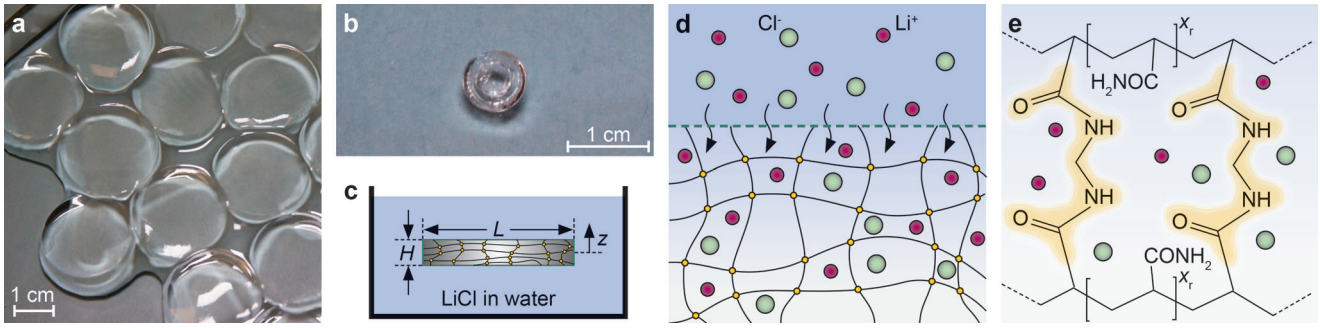

Figure 1. Loading polyacrylamide (PAM) hydrogels with salt by soaking the gel in an aqueous lithium chloride solution to form hygroscopic PAM–LiCl-composites. a) Typical PAM hydrogel disks in the wet state. b) PAM hydrogel disk in the dry state. c) Schematic of the swelling dynamics of a PAM hydrogel disk in an aqueous LiCl solution as a one-dimensional, transient mass transfer problem along the spatial coordinate, z. Progressive swelling of the gel in the salt solution increases the total disk thickness, H, and its diameter, L. d) Schematic illustration of the swelling process at the interface between the hydrogel and the salt solution. Along with the water, salt ions (Li^+ and Cl^- represented by red and green color, respectively) migrate into the polymer matrix thereby loading the gel with hygroscopic salt. e) Magnified, simplified schematic of the gel network showing the polymer chains that are connected via *N,N'*-methylenebisacrylamide crosslinkers to form a gel, where x_r represents the number of repeat units in between of crosslinks. After swelling in salt solutions, large amounts of ions will be present inside the gel.

swelling hydrogels in LiCl solutions is to achieve large contents of salt in the gel, which can then be translated into higher uptake when the hydrogels are used as sorbents, this increased swelling ratio of PAM is highly desirable and, as we will show later, can lead to exceptional water vapor uptakes.

By running the swelling experiments for extended durations, we were able to fully decouple the equilibrium swelling ratio from the swelling kinetics. This enables us to take a closer look at the swelling kinetics, which can be best observed in Figure 2b, where the relative sample weight is measured as a function of the swelling time. Here, we define relative sample weight as the current sample weight at the moment of the measurement divided by the final, equilibrium weight of the fully swollen sample. It becomes obvious that the more LiCl is added to the water, the slower the swelling kinetics. While the sample swelling in pure water reaches 90% of its equilibrium swelling ratio within less than 3 days, the sample in the saturated LiCl solution ($100\%_{sat}$) requires more than 30 days (720 h) to exceed this value. However, increasing the swelling temperature to 75 °C substantially enhances kinetics, which would be especially important in practical applications (see Figure S1, Supporting Information).

To better understand and predict the swelling dynamics, we model the salt loading process into the hydrogel by considering the free swelling of a thin hydrogel disk from its initial dry state to its fully swollen state in an aqueous LiCl solution. Figure 1c shows the modeled configuration. Since $L >> H$, the swelling process can be described as a 1D, transient mass transfer problem along the spatial coordinate, z. Due to the large swelling ratios observed in our experiments, we consider nonlinear swelling dynamics of a hydrogel where the concentration of solvent in the hydrogel and its mechanical stretch are coupled. In modeling our experiments, we consider the salt solution as a solvent that diffuses into the hydrogel and as such the hydrogel stretch in the z-direction, λ_2, is governed by a diffusion equation:[44]

$$\lambda_1^2 \frac{\partial \lambda_2}{\partial t} + 2\lambda_1 \lambda_2 \frac{\partial \lambda_1}{\partial t} = D \frac{\partial}{\partial z}\left(A \frac{\partial \lambda_2}{\partial z}\right) \tag{1}$$

where λ_1 is the stretch in the x- and y- directions, D is the effective diffusivity of the aqueous solution in the polymer network, and A is given by

$$A = \frac{1}{\lambda_1^2 \lambda_2^4} - \frac{2\chi\left(\lambda_1^2 \lambda_2 - 1\right)}{\lambda_1^4 \lambda_2^5} + \frac{N\Omega\left(\lambda_1^2 \lambda_2 - 1\right)\left(\lambda_2^2 + 1\right)}{\lambda_1^2 \lambda_2^4} \tag{2}$$

where χ is the Flory–Huggins chi parameter for the interaction between the PAM network and the aqueous solution, N is the effective number of polymer chains between crosslinks per unit volume of polymer, and Ω is the effective volume per mole of the solution.

The diffusivity D is taken as a variable due to the large variations in the polymer network as a consequence of the swelling: initially, when the solvent content in the hydrogel is small, the distance between polymer chains is small, limiting the diffusion of the solution. In contrast, at larger swelling ratios, there is more volume available for diffusion, leading to a higher D. Specifically, we follow the free volume theory to write:[45]

$$D = D_0 \left(1 - \frac{r_s}{\xi}\right) \exp\left(-\left(\frac{r_s}{r_{FVW}}\right)^3 \frac{\phi_p}{1 - \phi_p}\right) \tag{3}$$

where D_0 is the intrinsic diffusivity of the aqueous solution, taken here as a fitting parameter. r_s is the radius of the solute, r_{FVW} is the radius of the available free volume per molecule in the aqueous solution inside the hydrogel, ξ is the mesh size of the polymer network, and ϕ_p is the volume fraction of polymer. Due to the swelling process, the hydrogel mesh size ξ increases and the polymer volume fraction ϕ_p decreases. These two parameters evolve with the stretches as $\xi = \xi_\infty \left(\frac{\lambda_1^2 \lambda_2}{\lambda_\infty^3}\right)^{7/36}$ and $\phi_p = \frac{1}{\lambda_1^2 \lambda_2}$, where ξ_∞ is the mesh size of the hydrogel in its fully swollen, equilibrium state, and λ_∞ is the equilibrium stretch of the hydrogel,

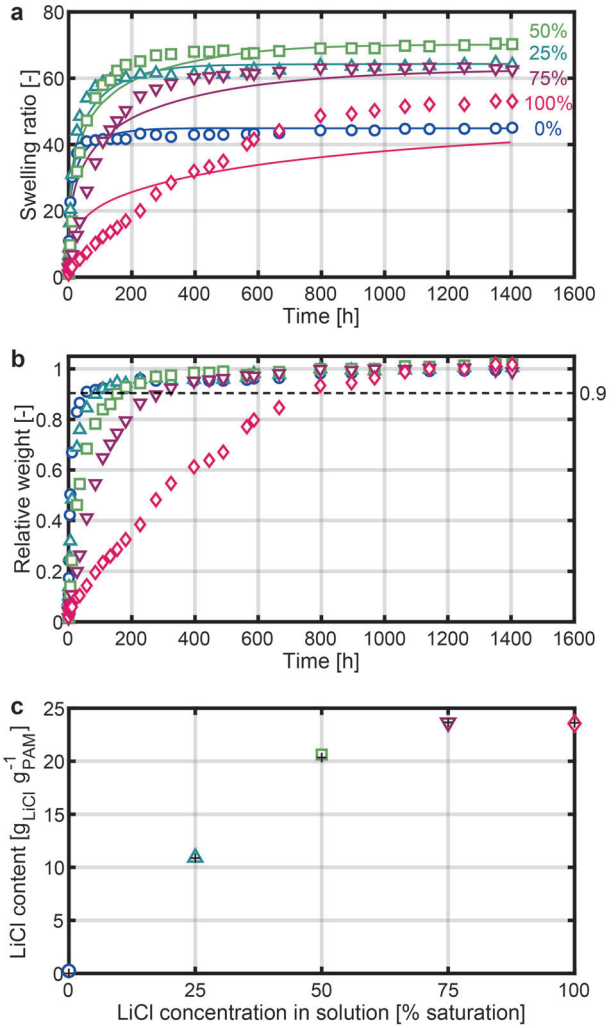

Figure 2. Swelling dynamics of PAM in aqueous LiCl solutions. a) Hydrogel swelling ratio, that is, current sample weight divided by initial, dried sample weight, as a function of swelling time. Symbols show measurements: Circles, upward-pointing triangles, squares, downward-pointing triangles, and diamonds represent swelling in 0%$_{sat}$, 25%$_{sat}$, 50%$_{sat}$, 75%$_{sat}$, and 100%$_{sat}$ solution, respectively. The solid lines represent our model results considering nonlinear diffusion of salt solution into the hydrogel. The swelling temperature was 23 °C. b) Relative sample weight, that is, current sample weight divided by the final, equilibrium sample weight, as a function of swelling time illustrating the PAM swelling kinetics for different LiCl concentrations in the aqueous solution. c) Salt loading at the end of the swelling process as a function of salt concentration in the swelling solution measured via thermogravimetric analysis (open symbols) and predicted based on salt concentration (black crosses).

considered isotropic.[44] The stretches λ_1 and λ_2 are coupled by the condition of no in-plane stresses in the hydrogel:[44]

$$\lambda_1^2 = \frac{1}{H}\int_0^H \lambda_2^2 dz \tag{4}$$

We solved Equations (1–4) to model the swelling dynamics in our experiments. Details of the boundary conditions used and the determination of the material properties N, ξ_∞, λ_∞ and χ based on mechanical characterization and swelling experiments are provided in Figure S2 and Table S1 (Supporting Information). From these material properties, we estimated the Flory–Huggins interaction parameters to be 0.49458, 0.48581, 0.48483, 0.49039, and 0.49648 for concentrations of 0%$_{sat}$, 25%$_{sat}$, 50%$_{sat}$, 75%$_{sat}$, and 100%$_{sat}$, respectively. Our calculated χ for PAM-water interaction agrees well with literature.[46] Additionally, χ was seen to have a non-monotonic dependence with the salt concentration highlighting the complex chemical interactions between water, salt ions, and polymer. The interaction parameter first decreased as the concentration increased showing a more favorable interaction between the polymer and the aqueous solution. This increased swelling in higher concentrations of LiCl in water has been previously attributed to the favorability of hydrogen bonding between the positive coordinated water molecules surrounding Li^+ ions and the electron pairs in the dipolar amide oxygen group in polyacrylamide.[43] However, close to the saturation limit, the interaction parameter increases, indicating a less energetically favorable interaction of the polymer with the concentrated salt solution, which we hypothesize could be a consequence of the favorability of hydration of the amide groups over cation binding to the polymers. Furthermore, the large, hydrated complexes formed around Li^+ will be entropically less favorable to mix with the polymer. These two factors translate into the solution acting as a poorer solvent.[43]

With the previous equations and experimentally characterized properties, we modeled the swelling dynamics in different salt concentrations. Our modeling results (see Figure 2a, lines) agree well with the experimental measurements (symbols), especially at low salt concentrations. We note that the values of the effective solution diffusivity, D_0, which were obtained from fitting the model to our experiments, show a consistent decrease as the salt concentration increases. This decreased diffusivity of the solution is well-correlated by the increased viscosity of the solution μ at higher saturation percentages, following a Stokes–Einstein behavior (D_0–μ^{-1}).[47] We show a plot of D_0 versus μ in Figure S3 (Supporting Information). We note that close to the saturation limit, the described model fails to accurately describe the observed swelling dynamics. We attribute this difference to be a consequence of the assumed physical picture of co-diffusion of salt and water into the polymer being less accurate for highly concentrated solutions.

Most importantly, we are swelling the PAM hydrogel disks in LiCl solutions in order to load them with the salt and enhance their hygroscopicity. We used thermogravimetric analysis (TGA) to assess the salt content of the PAM hydrogels after swelling to thermodynamic equilibrium in the different salt solutions. TGA is suitable for this task, since the thermal decomposition of the individual components of the LiCl-loaded PAM samples can be clearly decoupled when increasing the temperature from room temperature up to 800 °C (see Experimental Section, Supporting Information, on Thermogravimetric analysis and Figure S4, Supporting Information, for details).[48–50] In Figure 2c, we show the results as a function of LiCl concentration in the swelling solutions, where the salt content is defined as the mass of LiCl divided by the initial dry weight of the PAM sample. Overall, we demonstrate that extreme salt loadings are attainable. Swelling the gel in the 25%$_{sat}$, 50%$_{sat}$, 75%$_{sat}$, and 100%$_{sat}$ solutions yields salt contents of 10.9, 20.6, 23.6, and 23.6, respectively, showing a plateau

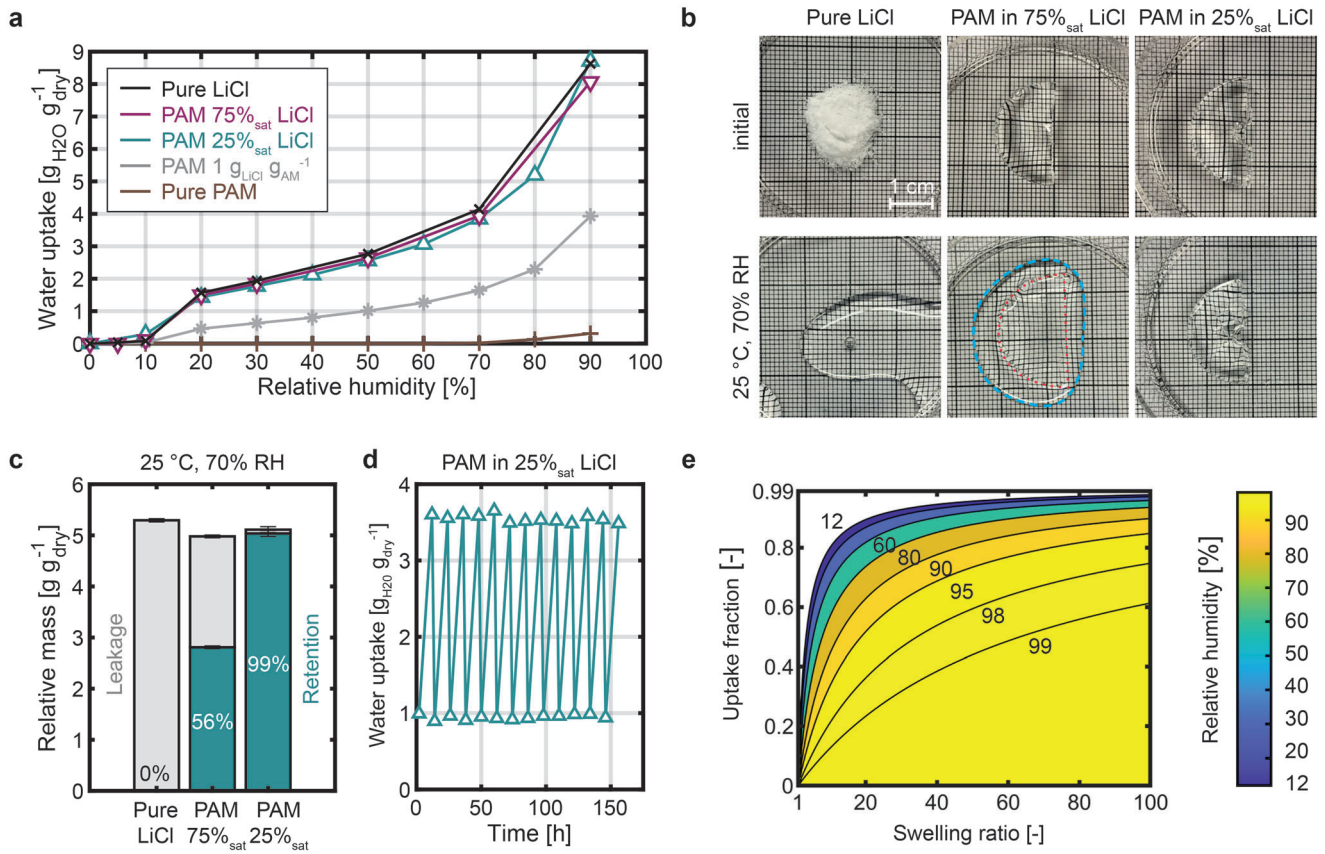

Figure 3. Performance of PAM hydrogels as a function of salt loading. a) Hygroscopicity measured with a dynamic vapor sorption device comparing the water uptake of pure LiCl to the uptake of a PAM hydrogel after swelling to equilibrate in an aqueous 75%$_{sat}$ and 25%$_{sat}$ LiCl solution, respectively, as well as pure PAM without salt and PAM where 1 g of LiCl per g of acrylamide (AM) was added during synthesis (see Experimental Section). Pure PAM and PAM 1 gg^{-1} LiCl were measured at 30 °C, while the other samples were measured at 25 °C. b) Examples of sorbents in their initial state (at the start of the experiment) versus their appearance when being equilibrated to an environment of 70% RH at 25 °C. The LiCl is initially in the as-received, dry state while the salt-loaded hydrogels are as-removed from their respective aqueous LiCl solution with 75%$_{sat}$ and 25%$_{sat}$, respectively. While the PAM hydrogel from the 25%$_{sat}$ LiCl solution does not show any leakage, both the pure LiCl and the PAM hydrogel from the 75%$_{sat}$ LiCl solution show substantial leakage. The red dotted line highlights the boundary of the hydrogel. The blue dashed line shows the leaked salt solution. c) Relative mass of the three samples in (b), defined as the mass in equilibrium divided by the dry mass of the samples. For pure LiCl the dry mass is measured, while for the salt-loaded hydrogels the mass is computed based on the results in Figure 2. We distinguish between the amount of salt solution that leaked out of the sample (gray) and the mass of the sample including the retained salt solution (turquoise). Percentages state the relative amount of retention. The error bars highlight the uncertainty of the measurement due to the precision of the scale. d) Stable water uptake of the PAM 25%$_{sat}$ LiCl during thermal cycling. Per cycle, the sample is exposed to 25 °C and 70% RH in an environmental chamber for 10 h (sorption) and to 70 °C in a dry oven for 2 h. The final amount of leaked salt solution is 3% of the total sample weight. e) Modeling results for the maximum allowable RH as a function material uptake fraction (compared to the uptake of pure LiCl) and swelling ratio, while avoiding leakage. The uptake fraction is determined by the amount of salt loading of the hydrogel. For higher swelling ratios, the hydrogel soaks in more salt solution, which during sorption leads to higher uptakes. For lower RH more salt can be loaded into the gel without causing leakage by using highly concentrated solutions.

in sample salt content for swelling solutions with concentrations above 75%$_{sat}$ (see Figure S5, Supporting Information, for SEM images of a dried LiCl-loaded PAM sample). These measured salt loadings agree with theoretical predictions. In equilibrium, given that the studied hydrogel is not a polyelectrolyte, we can assume that the salt concentration of the liquid inside the hydrogel is practically the same as the salt concentration of the surrounding swelling solution.[51] Based on this assumption, we also computed the amount of LiCl that was loaded into the hydrogel based on the equilibrium swelling ratio. In Figure 2c, we show these predictions. The deviation between measurement and prediction is less than 2% for all concentrations. These high salt loadings allow the hygroscopicity of the PAM–LiCl-composites to approach the pure LiCl limit and reach up to 96% of its uptake. However, as will be outlined next, a practical sorbent must also be able to retain all the water that it captures in order to avoid salt leakage.

2.3. Performance of Hygroscopic PAM–LiCl-Composites

We characterized the water sorption capabilities of the hygroscopic hydrogels by measuring their water uptake at different RH conditions using a dynamic vapor sorption (DVS) system (see Experimental Section for details). In **Figure 3**a, we show the uptake of PAM hydrogels after swelling to equilibrate in aqueous 75%$_{sat}$ and 25%$_{sat}$ LiCl solutions, respectively, and compare their

performance to pure LiCl, pure PAM without salt, as well as PAM where 1 g of LiCl per g of acrylamide (AM) was added before gelation via an alternative synthesis method (see Experimental Section). The PAM 75%$_{sat}$ LiCl sample shows an exceptional water uptake of 1.85, 2.64, and 3.94 gg^{-1} at RH of 30%, 50%, and 70%, respectively. These water uptakes correspond to 93–96% of the respective uptakes of pure LiCl, highlighting the extreme salt loading achieved of more than 20 g of salt per g of polymer, in agreement with Figure 2c. Based on the data in Figure 3a, we can confirm that the water uptake of these hygroscopic, non-polyelectrolyte hydrogels can be predicted from the sum of the weighted water uptakes of its constituents (i.e., pure LiCl and pure PAM). For the sample with the highest salt loading (PAM 75%$_{sat}$ LiCl), the deviation between measured uptake and prediction is less than 3% for all tested RH values (see Table S2, Supporting Information). Based on these DVS measurements, we could also show that sorption kinetics are similar between pure LiCl and the PAM 75%$_{sat}$ LiCl sample irrespective of relative humidity (see Figure S6, Supporting Information).

However, in addition to achieving high water uptake, hygroscopic hydrogels need to be designed to ensure that no leakage of the salt solution occurs, which is increasingly challenging for higher salt loadings of the hydrogel samples. Figure 3b shows the possible leakage for high concentration hydrogels in humid environments. Initially, dry lithium chloride and hydrogels swollen to equilibrium in 25%$_{sat}$ and 75%$_{sat}$ solutions were placed in an environmental chamber at a controlled temperature of 25 °C and a humidity of 70% for 48 h. Due to the high humidity, the different hygroscopic materials captured significant amount of water. Pure lithium chloride deliquesced and spread out in the container, highlighting the potential leakage issues that hygroscopic salts can have in practical sorption applications. Similarly, the hydrogel swollen in a 75%$_{sat}$ exhibited substantial leakage. We quantified the leakage by removing the hydrogel from the container and weighing the remaining solution, which corresponded to 44% of the total mass in the sample container (Figure 3c). We measured the salinity of the leaked solution to be 0.1666 g of LiCl per g of solution. This shows that along with water, there is a substantial amount of salt that leaks from the sample, highlighting the importance of mitigating leakage (see Supporting Information, Thermogravimetric Analysis). In contrast, a hydrogel prepared in a 25%$_{sat}$ solution did not show any observable leakage (Figure 3b), and the measured leaked liquid was only ≈1% of all the salt solution present. It is important to note that the measured amount of leakage is a conservative estimate. In fact, the measured mass remaining after removing the sample from its container is related to the retention of salt solution on the container surface as a result of detaching the sample from it. This analysis shows that leveraging the fundamental relationship between swelling, salt loading, water uptake, and leakage in hygroscopic hydrogels allows to enhance the uptake and prevent leakage while avoiding the need for encapsulation as proposed in the literature.[38]

In Figure 3d, we show results of thermal cycling of the PAM 25%$_{sat}$ LiCl sample. One cycle consisted of two steps. In step one, the sample was exposed for 10 h to 70% RH at 25 °C in an environmental chamber for vapor sorption. In step two, the sample was placed for 2 h in a dry oven at 70 °C for desorption. After 13 cycles, the final amount of leaked salt solution was 3% of the total sample weight, illustrating the cyclic stability of the material. The stable performance illustrates that water sorption, hydrogel swelling, and transport into the bulk of the material are compatible under the tested conditions. We confirmed the cyclic stability of our material further by performing dedicated cyclic DVS measurements (see Figure S7, Supporting Information).

Our leakage results can be interpreted by considering the equilibria of LiCl with water at varying RH and salt concentrations. At 75%$_{sat}$, the aqueous solution is at equilibrium with water vapor at 21% RH.[52] Therefore, a hygroscopic hydrogel with this concentration will capture more water if the ambient humidity is higher, which for hydrogels that have been swollen to their maximum volume causes the additional captured water to leak out of the hydrogel. In contrast, a 25%$_{sat}$ solution is at equilibrium at 75% RH.[52] Accordingly, a hydrogel containing aqueous solution with this concentration, will experience a minor loss of water due to the desorption at a 70% RH condition and consequently show no leakage.

Our previous analysis highlights the importance of choosing the appropriate salt concentration in the aqueous solution when loading hydrogels with salt. This concentration must be selected such that there is no leakage at the highest RH that the hydrogel will experience in its application, while also enabling an optimized salt loading. To simultaneously achieve these two goals, we propose the following steps: 1) The salt concentration that is at equilibrium with the highest application RH is chosen for the swelling of hydrogels. This concentration can be found with knowledge of the activity of the salt as a function of salt concentration or from an isotherm of the salt at different RH.[30,52] 2) Dried hydrogels are swollen in this aqueous salt solution. 3) During swelling, the mass of the hydrogels is monitored to ensure that the hydrogels reach equilibrium, and therefore, highest salt loading. The allowable RH during operation is a function of the salt loading and the swelling ratio of the hydrogels, as shown in Figure 3e (see also Figure S8, Supporting Information), where the water uptake fraction relative to LiCl was calculated assuming that the uptake is entirely due to the salt.[30,31] Low RH applications will be able to achieve uptakes increasingly closer to those of pure LiCl as higher salt concentrations can be used without a risk of leakage. For a given RH, the swelling ratio can be maximized to increase the water vapor uptake. Hydrogels with high swelling ratios will be able to capture more salt solution during swelling. As a consequence, the salt loading relative to the polymer will be higher and during sorption the water vapor uptake will be increasingly closer to that of LiCl. Practically, this can be achieved by tuning polymer chemistry to favor polymer-solution interaction,[53] or, as we show below, by freeze-drying or changing the hydrogel cross-linking density.[54] We note that Figure 3e represents a conservative estimate. By considering the maximum uptake to be expected at a given condition, our model safely provides a criterion to prevent leakage during practical operation.

2.4. Enhancing Sorbent Uptake and Comparison to Existing Sorbents

Following our previous insights to optimize water uptake by maximizing salt loading while preventing leakage, we focused on 25%$_{sat}$ lithium chloride solutions as hydrogels swollen in this solution will be leakage free up to RH = 75%. Specifically, we

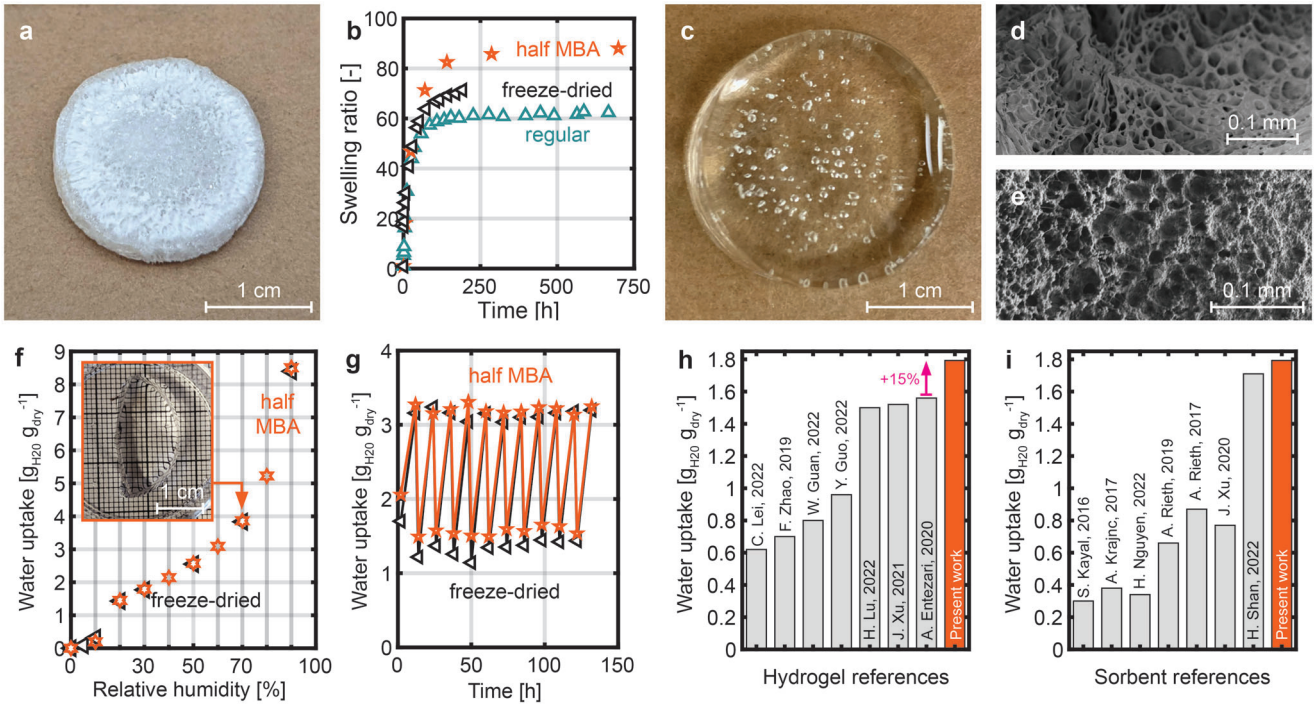

Figure 4. Maximizing water uptake of PAM–LiCl-composites. a) A freeze-dried PAM hydrogel disk. b) Swelling ratio versus swelling time for the freeze-dried sample and the less crosslinked, half MBA sample as compared to the regular crosslinked, oven-dried PAM sample when swelling in 25%$_{sat}$ LiCl solution. Freeze-dried and half MBA sample show an enhancement in equilibrium swelling ratio by 11% and 37%, respectively. c) An initially freeze-dried PAM disk after swelling to reach equilibrium with an aqueous 25%$_{sat}$ LiCl solution. d) Scanning electron microscopy (SEM) image of the PAM gel after freeze-drying showing the porous nature of the material. e) SEM image of the freeze-dried PAM gel after swelling to reach equilibrium with an aqueous 25%$_{sat}$ LiCl solution and subsequent thermal drying showing that the pores persist. f) Water uptake, defined as the amount of captured water divided by the dry weight of the sample, as measured by DVS for the half MBA and the freeze-dried sample. As verified in separate experiments, both samples show a water retention of more than 98% up to an RH of 70% (inset shows the half MBA sample when in equilibrium with an environment of 70% RH at 25 °C). g) Stable water uptake of the half MBA and freeze-dried sample during thermal cycling. Per cycle, the samples were exposed for 10 h to 70% RH at 25 °C in an environmental chamber (sorption) and to 70 °C in a dry oven for 2 h (desorption). The final amount of leaked salt solution was 3.6% and 0.9% of the total sample weight for the half MBA and the freeze-dried sample, respectively. h,i) Comparison of the water uptake of 1.79 gg^{-1} at 30% RH of the present work to other hydrogels and other sorbents in the literature, including the hydrogels presented by C. Lei et al.,[36] F. Zhao et al.,[34] W. Guan et al.,[56] Y. Guo et al.,[28] H. Lu et al.,[35] J. Xu et al.,[29] and A. Entezari et al.,[42] as well as the sorbents presented by S. Kayal et al. (zeolite),[55] A. Krajnc et al. (aluminophosphate),[57] H. Nguyen et al. (covalent organic framework),[58] A. Rieth et al. (MOF),[40] A. Rieth et al. (MOF),[41] J. Xu et al. (MOF),[59] and H. Shan et al. (LiCl in carbon felt).[60]

tested the swelling of freeze-dried PAM hydrogel samples as well as samples where only half the amount of MBA was used during synthesis (see Experimental Section; Figure S2, Supporting Information). We show a freeze-dried sample in **Figure 4**a, which looks substantially different to the oven-dried samples in the dried state (Figure 1b). In Figure 4b, we show the results of the swelling experiments performed in 25%$_{sat}$ LiCl solution. Compared to the standard, oven-dried sample (Figure 2a), the freeze-dried and, the half-MBA sample show an enhancement in equilibrium swelling ratio by 11% and 37%, respectively. In Figure 4c, we show the freeze-dried sample when fully swollen. We performed freeze-drying since this process led to microscopic pores and large internal areas in the samples (Figure 4d), which showed a net positive effect. While the pores trapped a few bubbles during swelling (Figure 4c), they accelerated the swelling kinetics due to the reduced diffusion distances and increased the equilibrium swelling ratio as LiCl solution can be captured and retained inside the hydrophilic pores. As shown in Figure 4e, these pores persisted after swelling in LiCl solution and thermal drying in an oven. We characterized the water uptake at different relative humidities at 25 °C of the freeze-dried and half-MBA PAM samples that were swollen to reach equilibrium with a 25%$_{sat}$ LiCl solution (Figure 4f). Both hydrogels exhibited high water uptakes. The freeze-dried samples exhibited high uptakes of 1.43, 1.77, 2.55, 3.84, and 8.40 gg^{-1} at an RH of 20%, 30%, 50%, 70%, and 90%, respectively, corresponding to 91–97% of the uptake of pure LiCl. The half MBA sample showed even higher uptakes of 1.45, 1.79, 2.58, 3.86, and 8.51 gg^{-1} at an RH of 20%, 30%, 50%, 70%, and 90%, respectively, corresponding to 93–99% of the uptake of pure LiCl, consistent with the salt loading of 16.6 g LiCl per g of polymer measured via TGA (see Supporting Information on Thermogravimetric analysis). We note that this salt loading is 52% higher than the loading of the oven-dried samples swollen in a solution with the same concentration (Figure 2), highlighting the role of reduced crosslinking in enhancing the swelling ratio. Most importantly, up to a relative humidity of 70%, there is negligible leakage of less than 1% that is resulting from the adhesion between the salt solution and the container surface during sample removal from the container (see Figure 4f, inset). In Figure 4g, we show results of thermal cycling of the two samples, with the

same protocol as discussed above (Figure 3d). After 10 cycles, the final amount of leaked salt solution was less than 4% of the total sample weight, illustrating the cyclic stability of the material.

The leakage-free equilibrium uptakes of the samples with reduced crosslinking exceed all previous hydrogels and sorbents demonstrated in literature. At 30% RH, our hydrogel provides a 15% increase in uptake compared to all previously fabricated hygroscopic hydrogels[42] owing to the exceptional salt loading and high hygroscopicity of LiCl (Figure 4h). Additionally, the uptake at 30% RH also exceeded all previously synthesized sorbents, where this uptake was over 2 times larger than the uptake of MOFs at the same conditions[41] and over 4 times larger than the uptake of zeolites[55] (Figure 4i).

3. Conclusion

We achieved record high water uptakes of hygroscopic hydrogels by attaining unprecedented swelling-induced salt loadings, which can exceed 20 g of LiCl per g of polymer. We characterized via experiments and models the swelling dynamics and equilibria of polyacrylamide in aqueous LiCl solutions with varying concentration, providing insights that guide the large salt loadings attained. By varying salt concentration and temperature of the swelling solution, cross-linking density of the hydrogel, drying protocols, and environmental sorption conditions, we established the fundamental relationship between swelling, salt loading, water uptake, and leakage in hygroscopic hydrogels. On this basis, we provided simple design guidelines to achieving hygroscopic hydrogels with maximized water uptake and with no leakage even at high relative humidity conditions. We fabricated leakage-free hydrogels with water uptakes of 1.79, 2.58, and 3.86 gg^{-1} at a RH of 30%, 50%, and 70%, respectively, exceeding previously reported water uptakes of hydrogels by 15% and water uptakes of MOFs by over 100%. This work is a significant step in the fabrication of high-performance sorbents for numerous applications such as atmospheric water harvesting, passive cooling, thermal energy storage, and space conditioning.

4. Experimental Section

Hydrogel Synthesis: Polyacrylamide (PAM) hydrogel based on a simple, one-pot approach was synthesized. At room temperature (23 °C), 100 g of deionized water was mixed with 8.36 g acrylamide (AM) monomer using a magnetic stirrer for 10 min until the monomer was fully dissolved. 5 mg *N,N′*-methylenebisacrylamide (MBA) as a crosslinker and 14.2 mg ammonium persulfate (APS) as initiator were added while continuously stirring. Finally, 12 µL *N,N,N′,N′*-tetramethylethylendiamin (TEMED) was added serving as accelerator, and the pre-gel solution was quickly filled into capped polypropylene vials (VWR, volume 15 mL) to cure at room temperature. During that process, the amount of air within the vials was minimized by filling the vials practically entirely. After 1 day of curing, a PAM hydrogel was formed that could be easily removed from the vials. Scissors were used to cut thin disks from the long, rod-like gel. The disks were stored in DIW until they were used for experiments. For the experiments shown in Figure 2, five disks (out of more than 100 hydrogel disks) were selected that possessed similar swollen mass (within ±2% deviation from the mean), which translates into disks of practically identical geometry. Subsequently, the disks were dried for 3 days at 60 °C in an oven at a RH of ≈0%. During the drying process, a spatula was used to prevent the disks from sticking to their substrate. As a result of drying, the disks lost more than 95% of their mass with a dry weight of 31 ± 1 mg (mean of the five disks ± standard deviation) and shrunk substantially. After sample preparation, the disks were swollen at room temperature (23 °C, if not stated otherwise) in aqueous LiCl solutions of varying concentrations, which were characterized based on percent saturation, where $100\%_{sat}$ represented a saturated aqueous LiCl solution that contained 83.2 g of LiCl per 100 g of DIW at 20 °C.[61] Free swelling of the hydrogel disks in pure DIW ($0\%_{sat}$), and in aqueous LiCl-solutions with $25\%_{sat}$, $50\%_{sat}$, $75\%_{sat}$, and $100\%_{sat}$ was studied. To track the swelling of the gels, the gels were briefly removed from the aqueous solutions to weigh them.

An alternative approach was also used to synthesize a LiCl-loaded PAM hydrogel. For a sample presented in Figure 3a, 8.36 g of LiCl was mixed into 100 g of deionized water leaving the solution cool down in a closed beaker. Subsequently, the standard recipe was prepared by adding 8.36 g AM, 5 mg MBA, 14.2 mg APS, and 12 µL TEMED. This resulted in a sample that contained a moderate, well-controlled amount of 1 g of LiCl per g of AM without the need of swelling in a LiCl solution, which served as a comparison to the regular samples.

To synthesize PAM samples with reduced crosslinking, the standard recipe, as outlined above, was used with the only difference that only half the amount of MBA (2.5 mg instead of 5 mg) was added. Further reducing the MBA content resulted in insufficient mechanical integrity of the swollen material.

Freeze-Drying: Freeze-drying was performed using a Labconco 7 934 000 Lyophilizer. Before freeze-drying, the hydrogel samples were frozen at −80 °C.

Scanning Electron Microscopy Characterization: SEM was conducted with a Zeiss Merlin high-resolution scanning electron microscope operated at 1 kV. Prior to imaging, hydrogel samples were freeze-dried and sputtered with a 5 nm coating of gold.

Dynamic Vapor Sorption Experiments: The sorption isotherms were characterized using the dynamic vapor sorption vacuum instrument (Surface Measurement Systems Ltd.). The samples were initially dried at 80 °C for 5 h, followed by a thermal equilibration at 25 °C for 3 h. The overall dehydration process was kept under a vacuum. Next, the mass of samples was recorded at a series of RH steps (from 0% to 90%) by regulating the partial pressure of water vapor at 25 °C. For sample equilibrium at each step of RH, an equilibrium criterion of $0.005\%_{sample}\ min^{-1}$, that is, a percentage change in sample mass per minute, was used to ensure precise measurement. For measurements at 90% RH, the measurements stopped at a maximum stage time of 2000 min.

Thermogravimetric Analysis: A Thermal Analysis System TGA/DSC 3+ by Mettler Toledo was used to measure the salt content of the hydrogels as well as the salinity of the leaked solution. Samples weighing ≈10 mg were placed into an inert alumina pan under nitrogen gas. At a slow rate of 1 K min^{-1}, the samples were heated up to 800 °C. For further details, see Supporting Information on Thermogravimetric analysis.

Statistical Analysis: To compute the swelling ratios, the measured sample weights during swelling were divided by the dry weight of the salt-free PAM before swelling. To compute the water uptake from the DVS measurements, the dry weight of the salt-containing PAM before sorption was subtracted from the measured sample weights during sorption. The resulting value was divided by the dry weight of the salt-containing PAM before sorption to obtain the water uptake in g per g of dry sorbent (PAM + LiCl).

Supporting Information

Supporting Information is available from the Wiley Online Library or from the author.

Acknowledgements

G.G. and C.D.D.M. contributed equally to this work. The authors thank the Office of Energy Efficiency and Renewable Energy for funding under grant no. DE-EE0009679. G.G. acknowledges funding by the Swiss National Science Foundation via a Postdoc Mobility grant (P400P2_194367). This work

made use of the MRSEC Shared Experimental Facilities at MIT, supported by the National Science Foundation under award number DMR-1419807. The authors thank Dr. Akshay Deshmukh for fruitful discussions.

Conflict of Interest

A patent has been filed on this work.

Data Availability Statement

The data that support the findings of this study are available from the corresponding author upon reasonable request.

Keywords

atmospheric water harvesting, hydrogel–salt composite, hygroscopic hydrogels, leakage, sorbents, sorption, thermoadsorptive energy storage

Received: December 16, 2022
Revised: May 12, 2023
Published online:

[1] M. M. Mekonnen, A. Y. Hoekstra, *Sci. Adv.* **2016**, *2*, e1500323.
[2] A. Boretti, L. Rosa, *npj Clean Water* **2019**, *2*, 15.
[3] H. Kim, S. Yang, S. R. Rao, S. Narayanan, E. A. Kapustin, H. Furukawa, A. S. Umans, O. M. Yaghi, E. N. Wang, *Science* **2017**, *356*, 430.
[4] H. Kim, S. R. Rao, E. A. Kapustin, L. Zhao, S. Yang, O. M. Yaghi, E. N. Wang, *Nat. Commun.* **2018**, *9*, 1191.
[5] A. LaPotin, Y. Zhong, L. Zhang, L. Zhao, A. Leroy, H. Kim, S. R. Rao, E. N. Wang, *Joule* **2021**, *5*, 166.
[6] N. Hanikel, M. S. Prévot, O. M. Yaghi, *Nat. Nanotechnol.* **2020**, *15*, 348.
[7] L. G. Gordeeva, Y. D. Tu, Q. Pan, M. L. Palash, B. B. Saha, Y. I. Aristov, R. Z. Wang, *Nano Energy* **2021**, *84*, 105946.
[8] J. Xu, J. Chao, T. Li, T. Yan, S. Wu, M. Wu, B. Zhao, R. Wang, *ACS Cent. Sci.* **2020**, *6*, 1542.
[9] C. Feng, P. Yang, H. Liu, M. Mao, Y. Liu, T. Xue, J. Fu, T. Cheng, X. Hu, H. J. Fan, K. Liu, *Nano Energy* **2021**, *85*, 105971.
[10] R. Li, Y. Shi, M. Wu, S. Hong, P. Wang, *Nat. Sustainability* **2020**, *3*, 636.
[11] C. Wang, L. Hua, H. Yan, B. Li, Y. Tu, R. Wang, *Joule* **2020**, *4*, 435.
[12] S. Pu, Y. Liao, K. Chen, J. Fu, S. Zhang, L. Ge, G. Conta, S. Bouzarif, T. Cheng, X. Hu, K. Liu, J. Chen, *Nano Lett.* **2020**, *20*, 3791.
[13] S. Narayanan, H. Kim, A. Umans, S. Yang, X. Li, S. N. Schiffres, S. R. Rao, I. S. McKay, E. N. Wang, C. A. Rios Perez, C. H. Hidrovo, *Appl. Energy* **2017**, *189*, 31.
[14] S. Narayanan, X. Li, S. Yang, H. Kim, A. Umans, I. S. McKay, E. N. Wang, *Appl. Energy* **2015**, *149*, 104.
[15] S. Narayanan, S. Yang, H. Kim, E. N. Wang, *Int. J. Heat Mass Transf.* **2014**, *77*, 288.
[16] W. O. Alabi, A. H. Karoyo, E. N. Krishnan, L. Dehabadi, L. D. Wilson, C. J. Simonson, *ACS Omega* **2020**, *5*, 9529.
[17] Y. Zhang, L. Wu, X. Wang, J. Yu, B. Ding, *Nat. Commun.* **2020**, *11*, 3302.
[18] D. Punwani, C. W. Chi, D. T. Wasan, *Ind. Eng. Chem. Process Des. Dev.* **2002**, *7*, 410.
[19] R. Li, Y. Shi, L. Shi, M. Alsaedi, P. Wang, *Environ. Sci. Technol.* **2018**, *52*, 5398.
[20] Q. N. Zhang, L. J. Zhao, S. H. Chen, X. Guo, Y. M. Luan, Y. H. Zhang, *Atmos. Environ.* **2021**, *247*, 118171.
[21] E. P. Ng, S. Mintova, *Microporous Mesoporous Mater.* **2008**, *114*, 1.
[22] J. M. Castillo, J. Silvestre-Albero, F. Rodriguez-Reinoso, T. J. H. Vlugt, S. Calero, *Phys. Chem. Chem. Phys.* **2013**, *15*, 17374.
[23] M. H. Simonot-Grange, *Clays Clay Miner.* **1979**, *27*, 423.
[24] M. Gwadera, K. Kupiec, *Adsorpt. Sci. Technol.* **2015**, *33*, 499.
[25] H. T. Chua, K. C. Ng, A. Chakraborty, N. M. Oo, M. A. Othman, *J. Chem. Eng. Data* **2002**, *47*, 1177.
[26] X. Liu, X. Wang, F. Kapteijn, *Chem. Rev.* **2020**, *120*, 8303.
[27] J. Canivet, A. Fateeva, Y. Guo, B. Coasne, D. Farrusseng, *Chem. Soc. Rev.* **2014**, *43*, 5594.
[28] Y. Guo, W. Guan, C. Lei, H. Lu, W. Shi, G. Yu, *Nat. Commun.* **2022**, *13*, 2761.
[29] J. Xu, T. Li, T. Yan, S. Wu, M. Wu, J. Chao, X. Huo, P. Wang, R. Wang, *Energy Environ. Sci.* **2021**, *14*, 5979.
[30] C. D. Díaz-Marín, L. Zhang, Z. Lu, M. Alshrah, J. C. Grossman, E. N. Wang, *Nano Lett.* **2022**, *22*, 1100.
[31] C. D. Díaz-Marín, L. Zhang, B. El Fil, Z. Lu, M. Alshrah, J. C. Grossman, E. N. Wang, *Int. J. Heat Mass Transf.* **2022**, *195*, 123103.
[32] R. Li, Y. Shi, M. Alsaedi, M. Wu, L. Shi, P. Wang, *Environ. Sci. Technol.* **2018**, *52*, 11367.
[33] G. Yilmaz, F. L. Meng, W. Lu, J. Abed, C. K. N. Peh, M. Gao, E. H. Sargent, G. W. Ho, *Sci. Adv.* **2020**, *6*, eabc8605.
[34] F. Zhao, X. Zhou, Y. Liu, Y. Shi, Y. Dai, G. Yu, *Adv. Mater.* **2019**, *31*, 1806446.
[35] H. Lu, W. Shi, J. H. Zhang, A. C. Chen, W. Guan, C. Lei, J. R. Greer, S. V. Boriskina, G. Yu, *Adv. Mater.* **2022**, *34*, 2205344.
[36] C. Lei, Y. Guo, W. Guan, H. Lu, W. Shi, G. Yu, *Angew. Chem., Int. Ed.* **2022**, *61*, e202200271.
[37] S. Aleid, M. Wu, R. Li, W. Wang, C. Zhang, L. Zhang, P. Wang, *ACS Mater. Lett.* **2022**, *4*, 511.
[38] R. Li, M. Wu, Y. Shi, S. Aleid, W. Wang, C. Zhang, P. Wang, *J. Mater. Chem. A* **2021**, *9*, 14731.
[39] T. Yan, T. Li, J. Xu, J. Chao, R. Wang, Y. I. Aristov, L. G. Gordeeva, P. Dutta, S. S. Murthy, *ACS Energy Lett.* **2021**, *6*, 1795.
[40] A. J. Rieth, A. M. Wright, G. Skorupskii, J. L. Mancuso, C. H. Hendon, M. Dincă, *J. Am. Chem. Soc.* **2019**, *141*, 13858.
[41] A. J. Rieth, S. Yang, E. N. Wang, M. Dincă, *ACS Cent. Sci.* **2017**, *3*, 668.
[42] A. Entezari, M. Ejeian, R. Wang, *ACS Mater. Lett.* **2020**, *2*, 471.
[43] Y. D. Livney, I. Portnaya, B. Faupin, O. Ramon, Y. Cohen, U. Cogan, S. Mizrahi, *J. Polym. Sci., Part B: Polym. Phys.* **2003**, *41*, 508.
[44] N. Bouklas, R. Huang, *Soft Matter* **2012**, *8*, 8194.
[45] E. Axpe, D. Chan, G. S. Offeddu, Y. Chang, D. Merida, H. L. Hernandez, E. A. Appel, *Macromolecules* **2019**, *52*, 6889.
[46] Polymerdatabase, https://polymerdatabase.com/polymerphysics/ChiTempdependence.html (accessed: December 2022).
[47] G. Peskir, *Stochastic Models* **2003**, *19*, 383.
[48] A. K. Bhattacharya, A. Hartridge, K. K. Mallick, *J. Mater. Sci.* **1997**, *32*, 1113.
[49] P. J. Masset, *J. Therm. Anal. Calorim.* **2009**, *96*, 439.
[50] J. D. Van Dyke, K. L. Kasperski, *J. Polym. Sci., Part A: Polym. Chem.* **1993**, *31*, 1807.
[51] G. Chen, *Phys. Chem. Chem. Phys.* **2022**, *24*, 12329.
[52] M. R. Conde, *Int. J. Therm. Sci.* **2004**, *43*, 367.
[53] Y. Zhou, L. Jin, *Soft Matter* **2020**, *16*, 5740.
[54] R. Subramani, A. Izquierdo-Alvarez, P. Bhattacharya, M. Meerts, P. Moldenaers, H. Ramon, H. Van Oosterwyck, *Front. Mater.* **2020**, *7*, 212.
[55] S. Kayal, S. Baichuan, B. B. Saha, *Int. J. Heat Mass Transf.* **2016**, *92*, 1120.
[56] W. Guan, C. Lei, Y. Guo, W. Shi, G. Yu, *Adv. Mater.* **2022**, https://doi.org/10.1002/adma.202207786.
[57] A. Krajnc, J. Varlec, M. Mazaj, A. Ristić, N. Z. Logar, G. Mali, *Adv. Energy Mater.* **2017**, *7*, 1601815.

[58] H. L. Nguyen, C. Gropp, N. Hanikel, A. Möckel, A. Lund, O. M. Yaghi, *ACS Cent. Sci.* **2022**, *8*, 926.
[59] J. Xu, T. Li, J. Chao, S. Wu, T. Yan, W. Li, B. Cao, R. Wang, *Angew. Chem., Int. Ed.* **2020**, *59*, 5202.
[60] H. Shan, C. Li, Z. Chen, W. Ying, P. Poredoš, Z. Ye, Q. Pan, J. Wang, R. Wang, *Nat. Commun.* **2022**, *13*, 5406.
[61] *Ullmann's Encyclopedia of Industrial Chemistry*, Wiley, Hoboken, NJ, USA **2003**.